Electronic Supplementary Information

Defect Mitigation using D-Penicillamine for Efficient Methylammonium-Free Perovskite Solar Cells with High Operational Stability

Jianchao Yang,‡[ab] Weijian Tang,‡[a] Ruihan Yuan,[a] Yu Chen,[a] Jing Wang,[c] Yihui Wu,*[a] Wan-Jian Yin,*[c] Ningyi Yuan,[b] Jianning Ding,*[bd] and Wen-Hua Zhang*[a]

[a] Sichuan Research Center of New Materials, Institute of Chemical Materials, China Academy of Engineering Physics, 596 Yinhe Road, Shuangliu, Chengdu 610200, China

E-mail: yihuiwu@caep.cn; whzhang@caep.cn

[b] Jiangsu Collaborative Innovation Center of Photovoltaic Science and Engineering, Changzhou University, Changzhou, 213164, China

E-mail: dingjn@cczu.edu.cn

[c] College of Energy, Soochow Institute for Energy and Materials InnovationS (SIEMIS), Soochow University, Suzhou, 215006, China

E-mail: wjyin@suda.edu.cn

[d] Micro/Nano Science and Technology Center, Jiangsu University, Zhenjiang 212013, China

‡ These authors contributed equally to this work.

Materials: All the chemicals were used as received. Lead iodide (≥98%, TCI, Tokyo Chemical Industry); Cesium iodide (≥99.9%, Sigma-Aldrich); Lead bromide and Lead Chlorine (≥98%, Sigma-Aldrich); $HC(NH_2)I$ (FAI), $HC(NH)_2Br$ (FABr), spiro-OMeTAD and PTAA were purchased from Xi'an p-oled. D-Penicillamine (99%) was purchased from alfa. All of the solvents were purchased from Aladdin and used without purification. In addition, the FTO was purchased from Beijing Huamin New Materials Technology Co. Ltd. (The sheet resistance was 14 ohm and the thickness was 2.2 mm).

Device fabrication: All devices were prepared on the cleaned and patterned FTO substrates. The compact TiO_2 layer was fabricated using hydrothermal treatment of 0.2 M $TiCl_4$ at 70 ^oC for 1 h. The resultant films were washed with ethanol, deionized water and then annealed at 150 ^oC for 30 min. Perovskite film was deposited by a green anti-solvent processed spin coating method in a nitrogen-filled glovebox. The precursor solution for the narrow bandgap perovskite (~1.56 eV) is comprised of 52 mg of CsI, 186 mg of FAI, 8 mg of FABr, 591 mg of PbI_2, 18 mg of $PbCl_2$ in 1 mL of dimethyl formamide (DMF) and dimethylsulfoxide (DMSO) (4:1, v/v). The wide-bandgap perovskite (~1.73 eV) precursor solution is comprised of 52 mg of CsI, 128 mg of FAI, 50 mg of FABr, 436 mg of PbI_2, 150 mg of $PbBr_2$. For the PA containing samples, the concentration of PA was tuned in the range of 0-0.1 mg/mL.

For the small area solar cells (narrow- and wide-bandgap devices), the precursor solution was deposited on compact TiO_2 substrates by a consecutive two-step spin-coating process at 1000 and 5000 rpm for 10 and 40 s, respectively. 130 μL of anisole was dropped onto the substrate at 20 s before the end. And then the wet film was annealed at 110 ^oC for 20 min.

For the mini module, a vacuum quenching-assisted method was adopted. The mini module was fabricated on an FTO substrate (4 × 4 cm^2). Firstly, the FTO substrate was etched by laser ablation to remove the conducting layer (P1), as shown in Fig. S16. Secondly, the compact TiO_2 was deposited by a hydrothermal approach, with parts of the FTO covered by adhesive tape. Then, the substrate was moved to a glovebox. The narrow bandgap perovskite solution was spin-coated onto the compact TiO_2 substrates at 4000 rpm for 10 s. Then, the wet film was transferred into a stainless-steel chamber connected to a rotary vane vacuum pump and covered with quartz glass. When the color of the wet film changed, the vacuum pump was turned off immediately. The film was subsequently transferred to a hotplate and annealed at 110 °C for 20 min. The vacuum quenching-assisted equipment was consisting of three part: a self-made vacuum sucker, an electromagnetic valve (Hongke Vacuum Valve Technology Co.

LTD. Mode number: GDC-J16A), a vacuum pump (Hengshui Motor Co. LTD, Mode number: YE2-80M2-2). Please see Fig. S15 and S16.

When the perovskite film was cooled to room temperature, a solution of spiro-OMeTAD/chlorobenzene (72.3 mg mL^{-1}) was spin coated onto perovskite films at 5000 rpm for 30 s in glove box, where 28.8 μL of 4-tert-butylpyridine and 17.5 μL of Li-TFSI/acetonitrile (520 mg mL^{-1}) were used as the additive. The spiro-OMeTAD solution was stirred for 2 h in a N_2-filled glovebox before use. Finally, 100 nm of gold electrodes were deposited by thermal evaporation. And then the device was immediately tested to acquire the *J-V* curves.

For PTAA-based devices, the PTAA (Mw = 20000, Xi'an Polymer Light Technology Corp.) solution was spin-coated onto perovskite films at 4000 rpm for 30s, in which the PTAA solution was prepared by dissolving 20 mg of PTAA, 15 μL of TPFB (4-isopropyl-4'-methyldiphenyliodonium tetrakis (pentafluorophenyl)borate, TCI Co. Ltd.)/acetonitrile (100 mg/mL) into 1 mL of chlorobenzene. This solution was also stirred for 2 h in a N_2-filled glovebox before use.

Characterization: The top-viewed and the cross-sectional SEM images were obtained by using a Hitachi SU8020 field-emission scanning electron microscopy (Hitachi High Technologies Corporation). AFM was recorded from Dimension V. The UV-Visible absorption spectra of the solution and thin films were measured from the absorbance model (without integrating sphere) using an Evolution™ 201 spectrophotometer (Thermo fisher scientific Corporation) with a scaning rate of 600 nm/min in the range of 800-300 nm at a step bandwidth of 1 nm. The type of baseline calibration was the 100% transmittance baseline. The XRD patterns of the perovskite films were recorded on Maxima 7000 diffractometer (Shimadzu, Japan) with a Cu Kα radiation (40 kV, 100 mA) and a scaning rate of 5°/ min in the 2θ range of 5-70° at a step size of 0.02 s. The steady PL spectra and time-resolved PL decay measurements were performed using an HORIBA DeltaFlex system (HORIBA). For the TRPL measurement, an excitation wavelength at 510 nm was used. Repetition rate were 100 MHz and 2 MHz, respectively. All perovskite films were deposited on quartz substrate.

The current-voltage characteristics were measured by Keithley 2400 source and the solar simulator with standard AM 1.5G (100 mW/cm^2, SSF5-3A: Enlitech) under ambient conditions. The *J-V* curves were measured by forward (-0.1 V to 1.2 V forward bias) or reverse (1.2 V to -0.1 V) scans with a delay time of 100 ms for each point. For the wide-bandgap PSCs, the scaning range of the voltage is from -0.1 V to 1.5 V or 1.5 V to -0.1 V.

The *J-V* curves for all small area devices were obtained by masking the cells with a metal mask 0.09 cm^2 in area.

The devices for long-term stability measurement were stored under ambient air conditions (RH: ~35%, RT). After various periods of time, the devices were removed from the desiccator and measurements were performed.

The operational stability with light soaking was carried out in N_2-filled glovebox under ~1 sun continuous illunination (white light LED) with temperature of ~30 ^oC, the *J-V* curves were in-situ, automatically collected every 10 s to track the MPP.

The devices for thermal aging were placed on a 85 ^oC hotplate in a N_2 filled glovebox. For *J-V* testing, the device was removed from the hotplate periodically and measurements were performed.

Monochromatic external quantum efficiency (EQE) spectra were recorded as functions of wavelength with a monochromatic incident light of 1 x 10^{16} photons cm^{-2} in alternating current mode with a bias voltage of 0 V (QE-R3011). The light intensity of the solar simulator was calibrated by a standard silicon solar cell provided by PV Measurements. Electrochemical impedance spectroscopy (EIS) was obtained by using a multi-channel potentiostat (VMP3, Biologic) under dark conditions in the frequency range from 1 MHz to 100 mHz with an AC amplitude of 30 mV. Mott-Schottky analysis were conducted by using a multi-channel potentiometer (VMP3, Biologic) at the frequency of 50 KHz in the applied voltage range from 0 V to 1.5 V with an AC amplitude of 25 mV. A Fourier transform infrared spectroscopy (FT-IR, TENSOR 27) was used to collect the FT-IR spectral data for the samples without and with PA. The sample was coated on KBr pellet. The liquid state ^{1}H nuclear magnetic resonance (NMR) measurements were recorded on Bruker AVANCE AV II 500 MHz spectrometer (TMS as an internal standard ($\delta = 0$)). UPS and XPS spectra were recorded by a Thermo-Fisher ESCALAB 250Xi system. For XPS measurement, radiation was produced by a monochromatic 75 W Al Kα excitation centred at 1486.7 eV. For UPS measuremnt, He I ultraviolet radition source of 21.2 eV was used.

Theoretical simulations

All calculations were carried out using density functional theory (DFT) as in implemented in the Vienna *ab* initio Simulation Package (VASP) program. The interaction between the core and valence electrons for all atoms in the system was described using the projector augmented wave (PAW) approach. The generalized gradient approximation (GGA) of the Perdew-Burke-Ernzerhof (PBE) functional was used for the exchange correlation functional. In order to avoid the interaction of neighboring junctions, the periodic images were separated along the surface direction by a vacuum thickness of 20 Å. The kinetic energy cutoff of the plane-wave basis was set to 300 eV. The crystal structure was fully relaxed until the convergence criteria of total energies and atomic forces were less than 1x10^{-4} eV and 0.02 eV/Å, respectively. For structural optimization, a 1x1x1 Monkhorst-Pack *k*-point mesh has been adopted, while the electronic structure calculations were carried out with a denser 3x3x1 mesh.

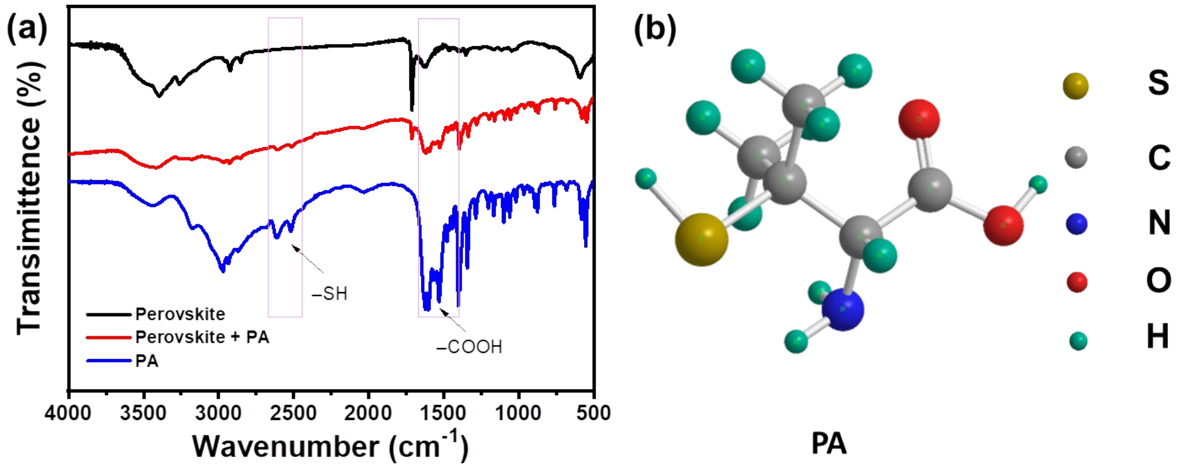

Fig. S1 (a) FTIR spectra of PA, perovskite, and PA containing perovskite samples. (b) The structural formula of PA molecule.

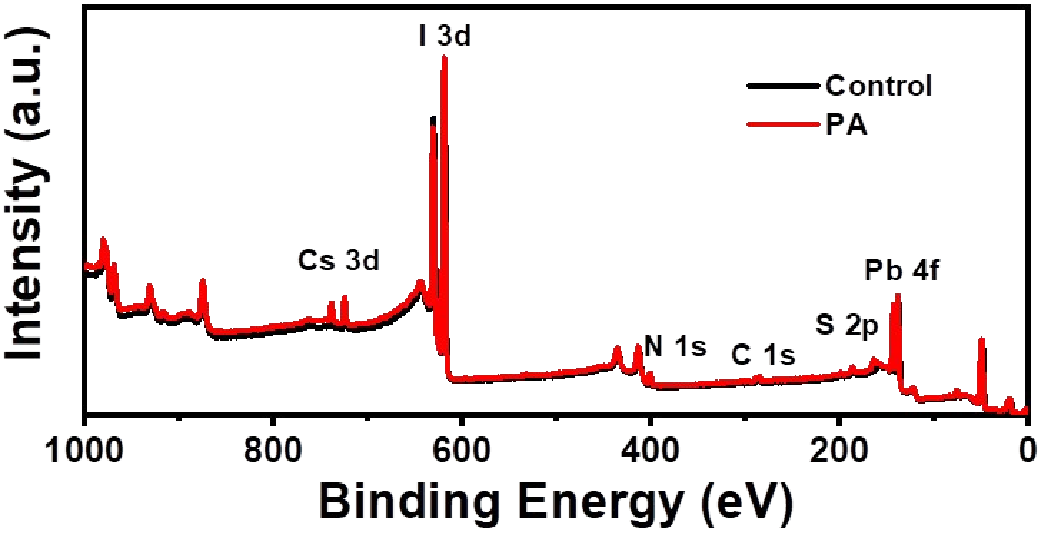

Fig. S2 The survey XPS spectra of the control and PA containing perovskite films.

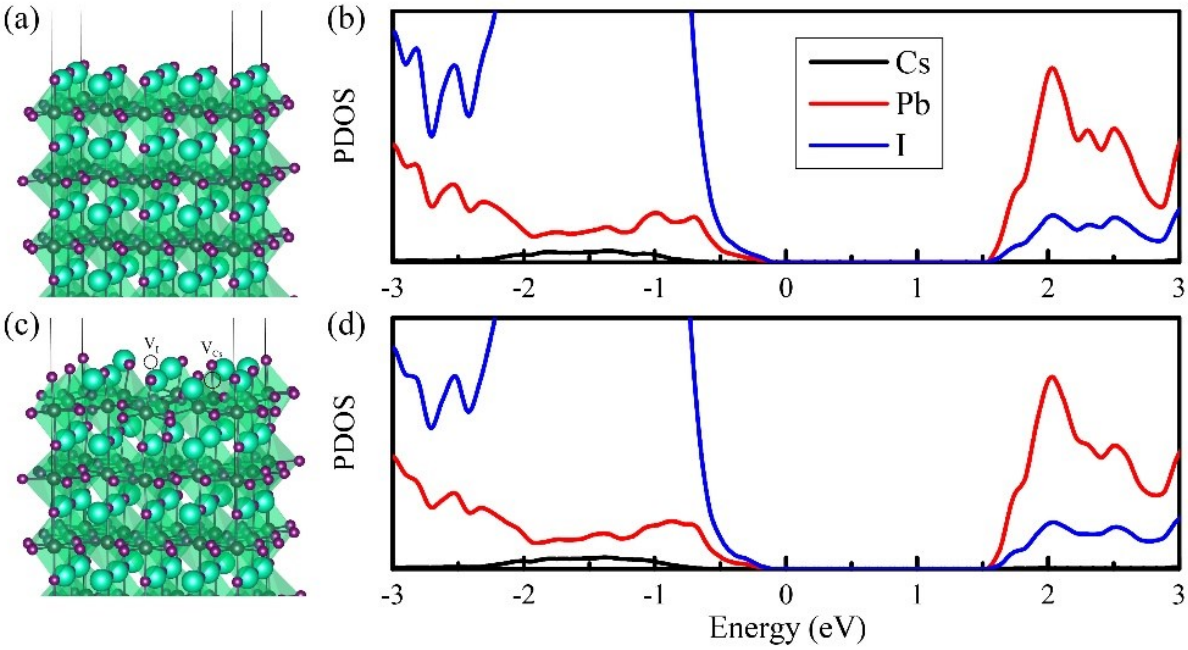

Fig. S3 Optimized geometry (a, c) and projected density of states (b, d) of the perfect perovskite and the same surface (001) with both V_I and V_{Cs} created by removing the iodine, and lead atoms colored in black in part. These two structural systems create no gap states.

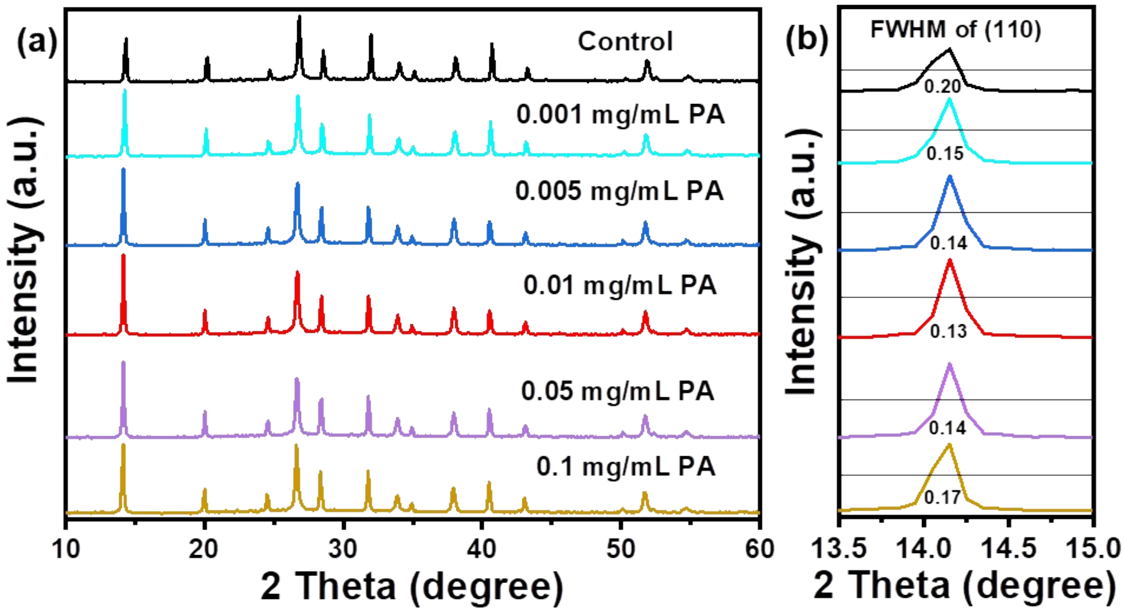

Fig. S4 (a) XRD patterns of perovskite films with different PA concentrations and (b) the corresponding full width at half maximum (FWHM) of (110) diffraction peak.

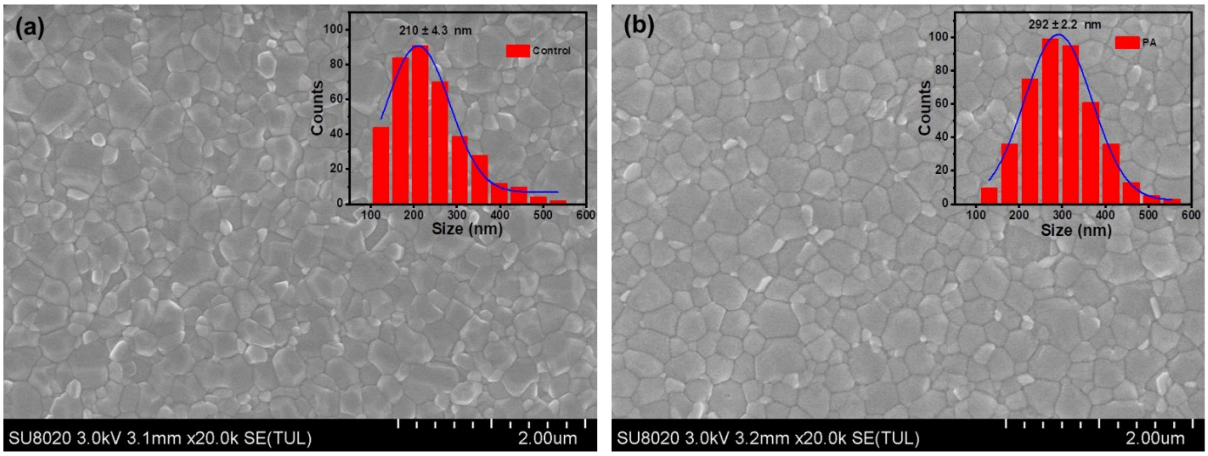

Fig. S5 SEM images of perovskite films without (a) and with (b) PA (inset: the corresponding grain size distribution).

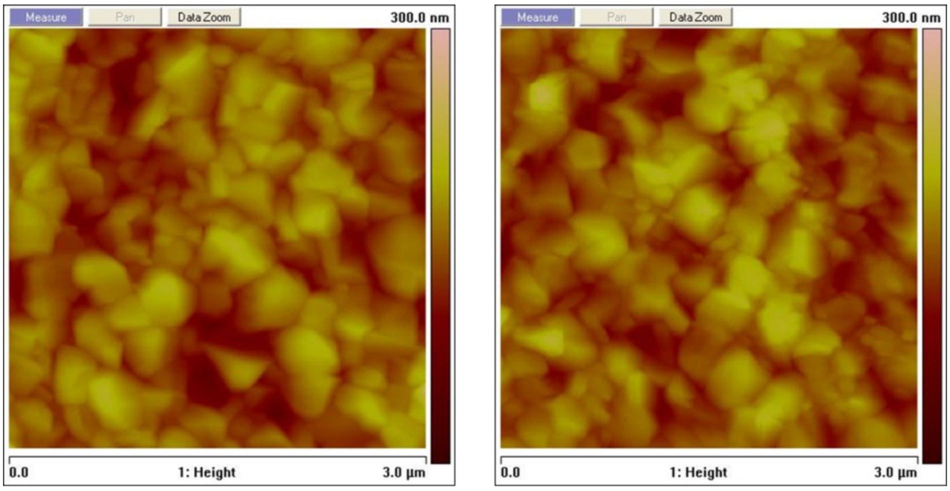

Control

PA

Fig. S6 The root-mean-square (RMS) roughness of the control and PA containing perovskite films measured from AFM.

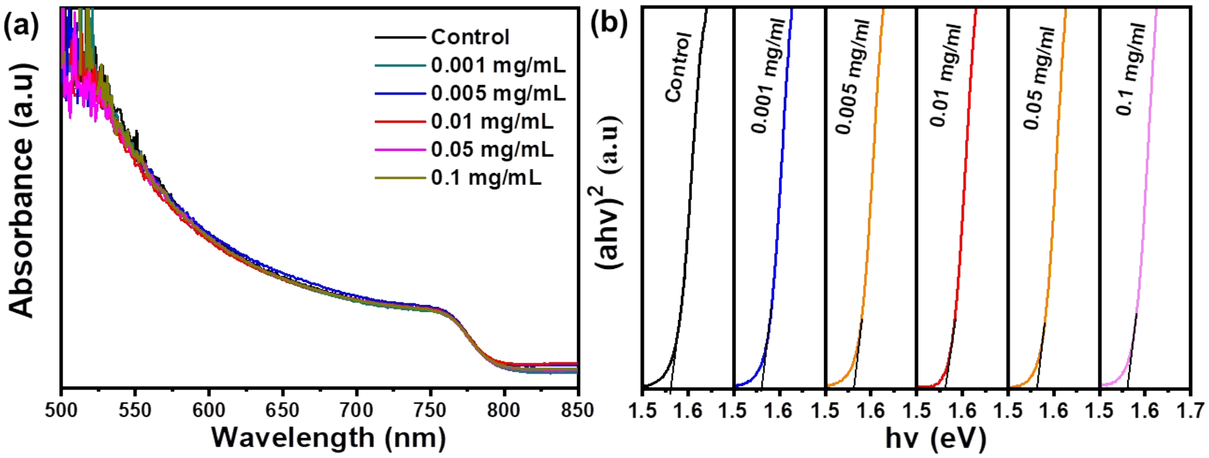

Fig. S7 (a) The UV-vis absorption spectra of perovskite films with different PA concentrations and (b) the corresponding bandgaps (1.56 eV).

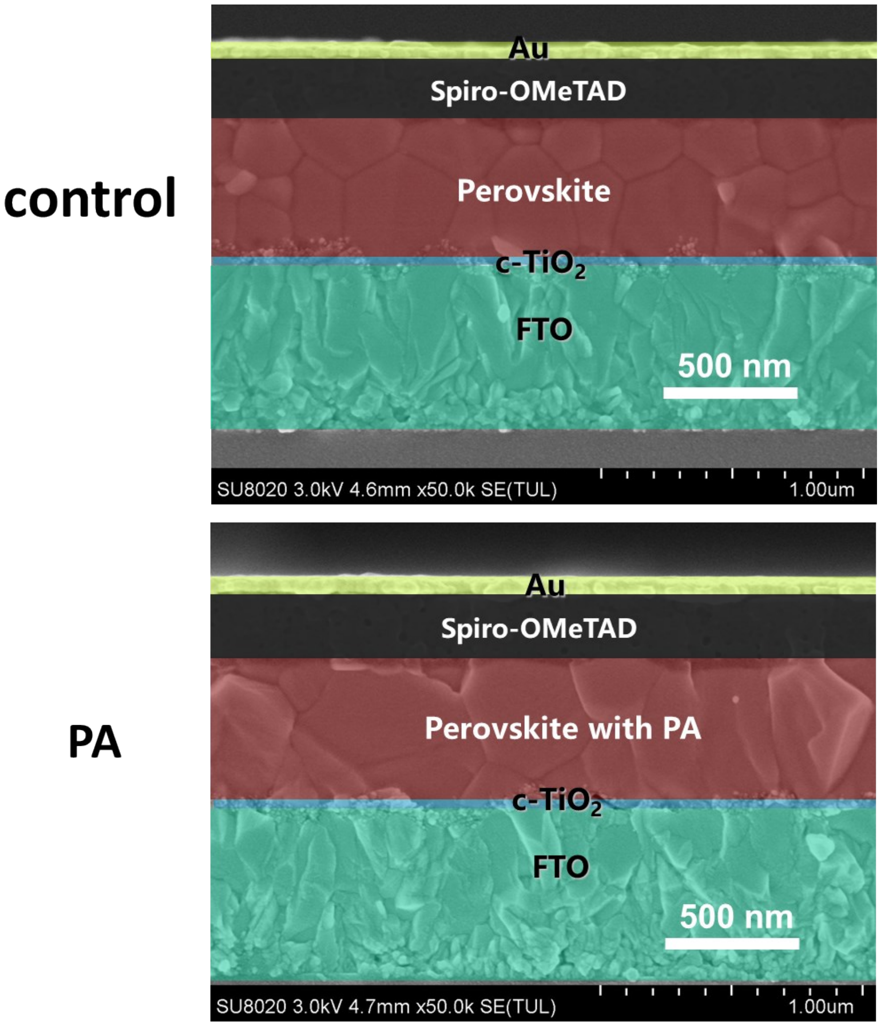

Fig. S8 Typical cross-sectional SEM images of the control and PA containing PSCs.

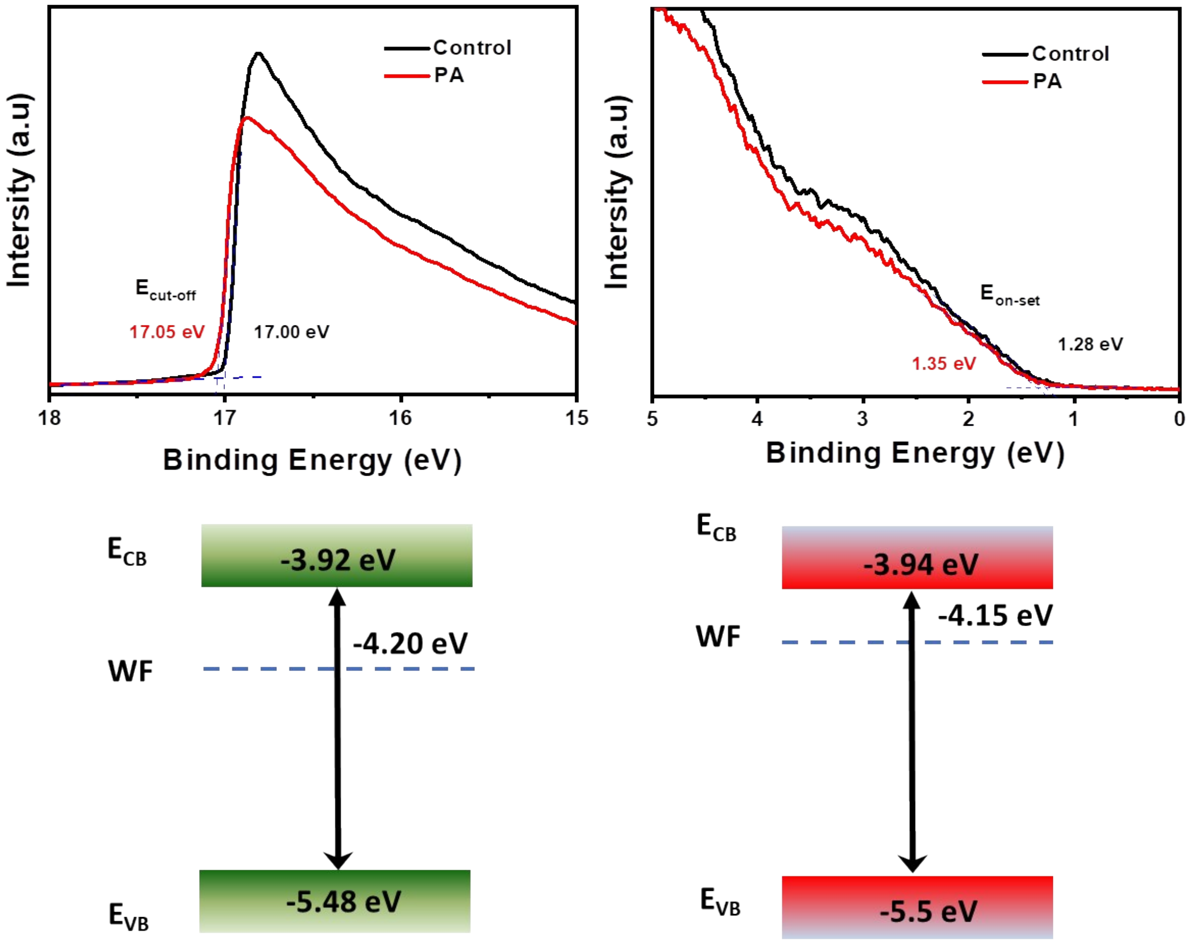

Fig. S9 The UPS spectra of the perovskite films without and with PA, and the corresponding energy levels.

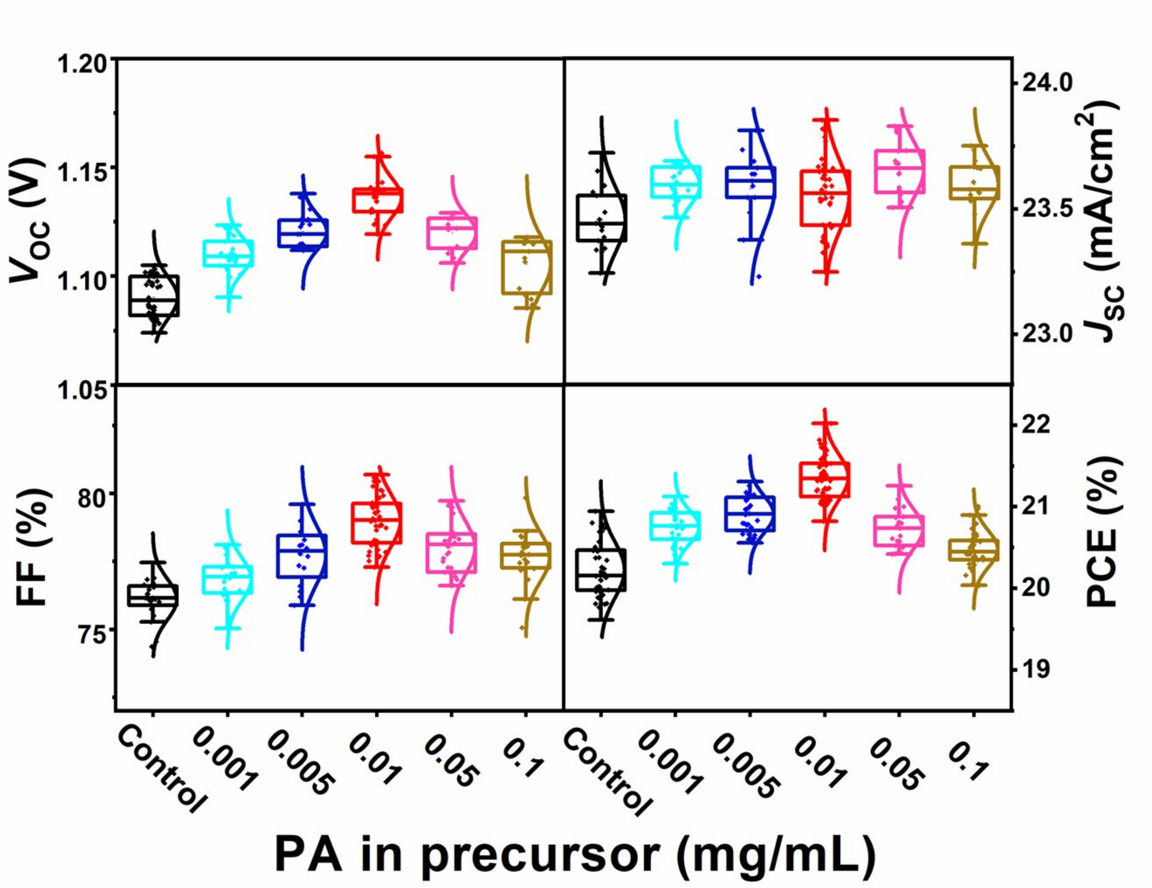

Fig. S10 Statistics of PV parameters (V_{OC}, J_{SC}, FF, and PCE) for the devices based on the perovskite films with different PA concentrations.

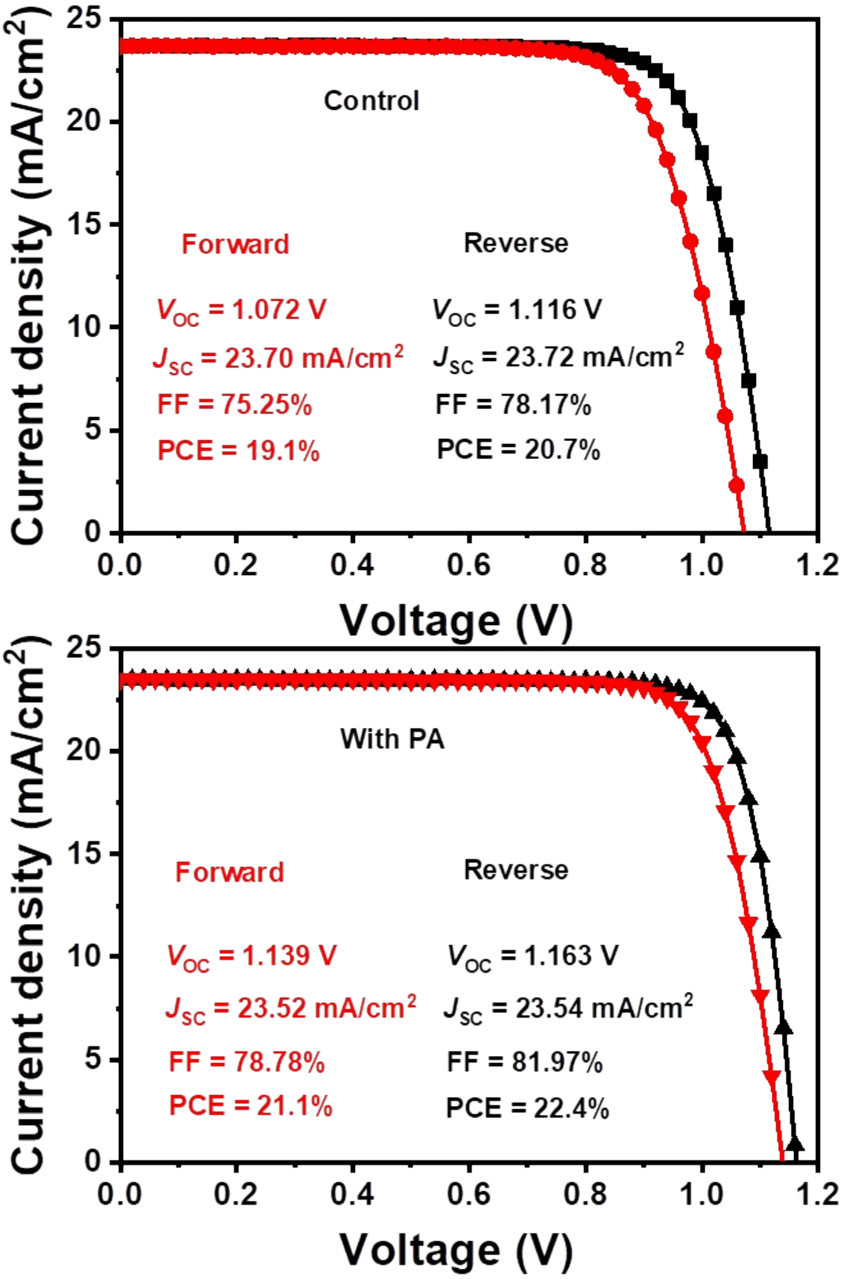

Fig. S11 Hysteretic effect of the devices based on the control and PA containing perovskite films.

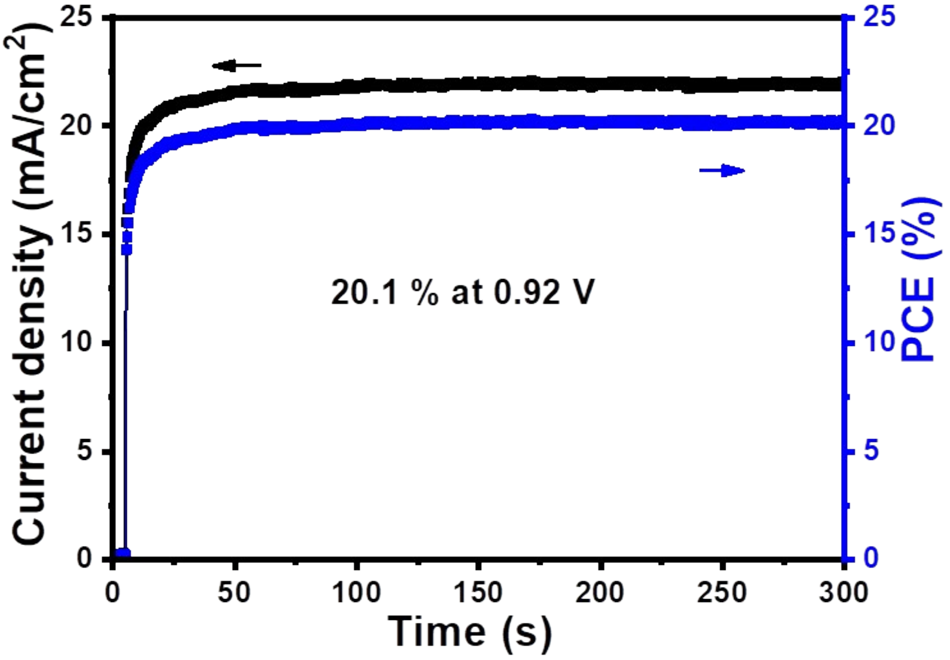

Fig. S12 Stabilized output efficiency of the control device around the maximum output power point a function of time under simulated 1 sun illumination.

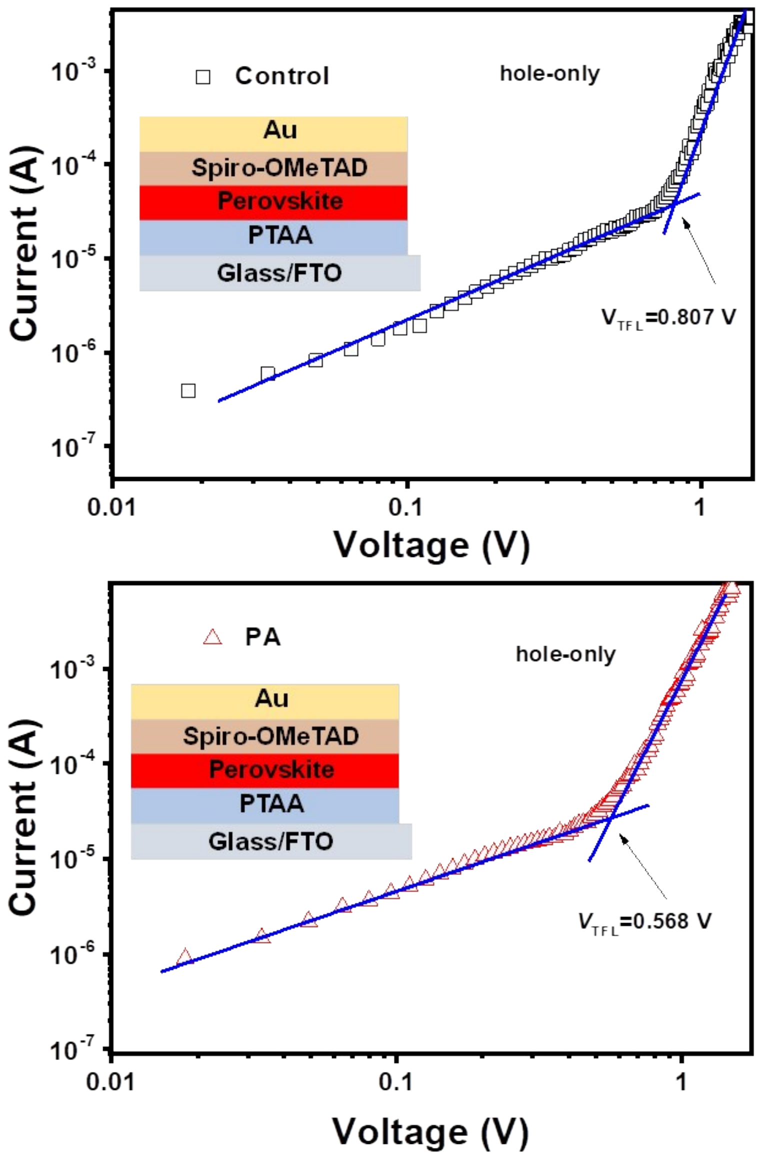

Fig. S13 Dark current-voltage curves for the hole-only structured devices with control and PA containing perovskite, respectively

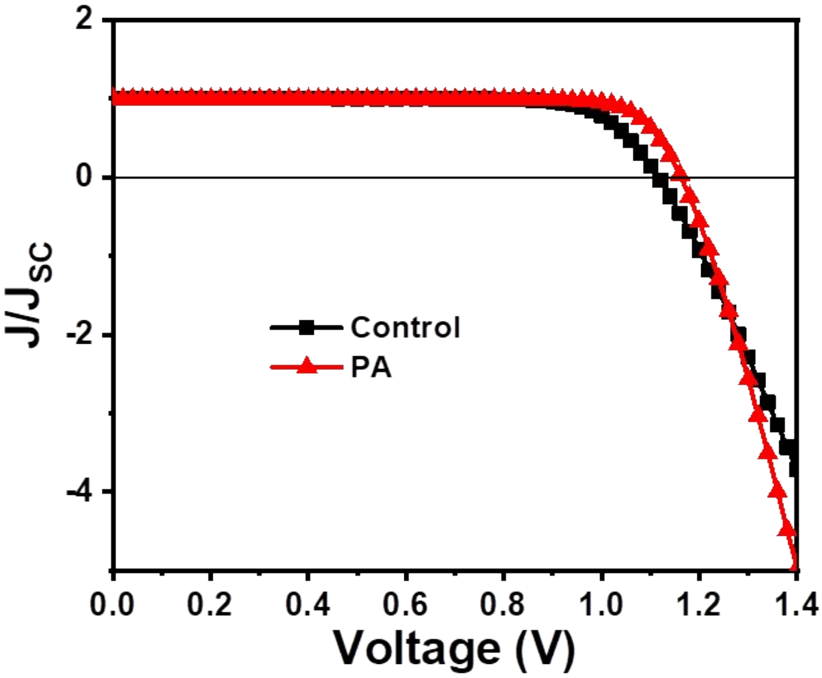

Fig. S14 The normalized *J-V* curves of the control and PA containing devices.

Fig. S15 The photographs of a self-made vacuum sucker (left) and the model number of the vacuum pump (right) for the vacuum quenching-assisted method.

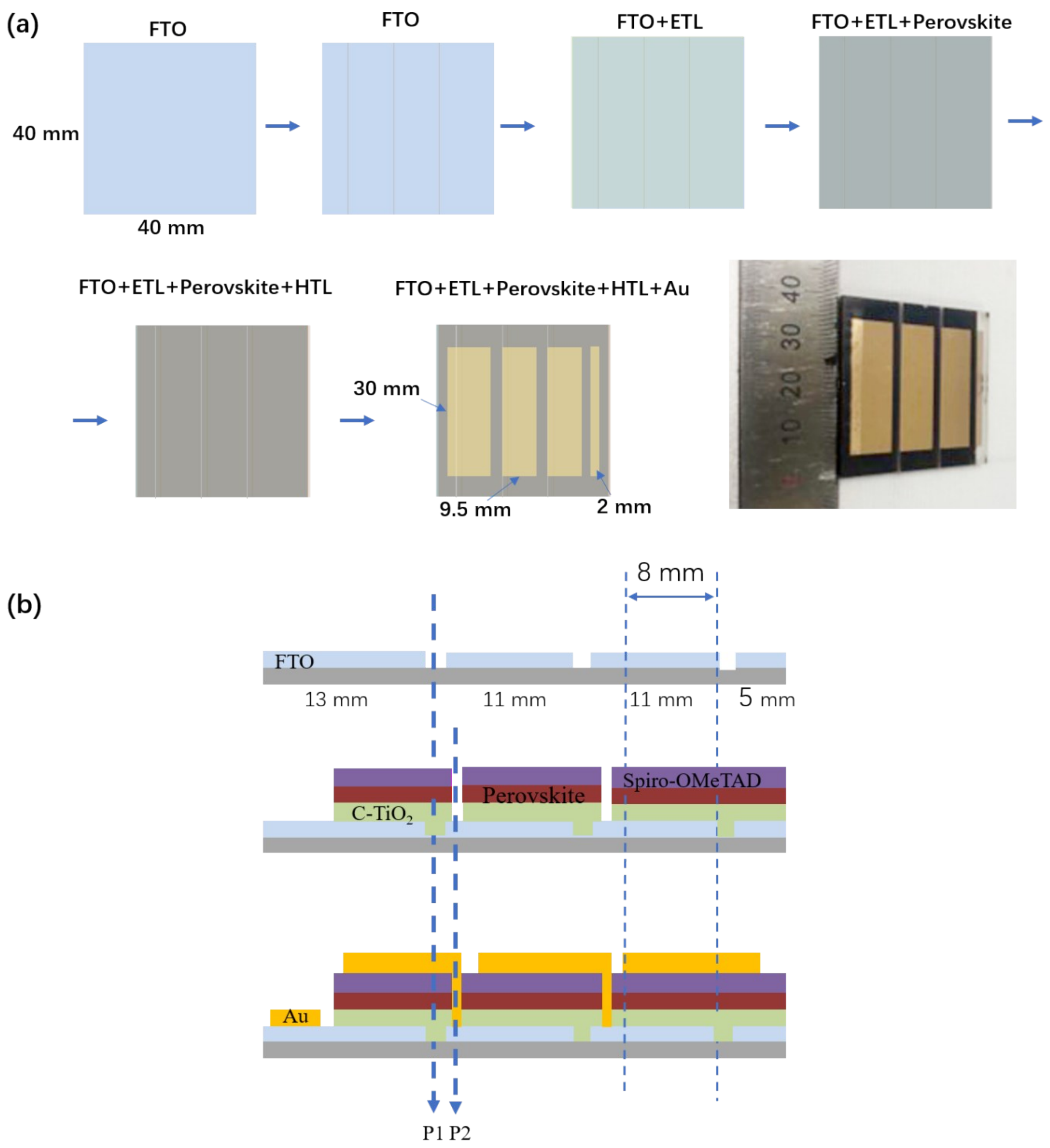

Fig. S16 (a) The fabrication process and (b) device scribing structure for the large-area PSCs.

Table S1. Recently progresses in MA-free, Cs/FA-based PSCs with normal structures.

Year	Device structures	Scan direction	V_{OC} (V)	J_{SC} (mA cm^{-2})	FF (%)	PCE (%)	Ref
2015	FTO/c-TiO_2/$\mathbf{Cs_{0.1}FA_{0.9}PbI_3}$/Spiro/Ag	Re	1.07	23.4	75.9	19.0	1
		Fw	1.04	23.6	56.7	13.9	
2016	FTO/c-TiO_2/$\mathbf{Cs_{0.15}FA_{0.85}PbI_3}$/Spiro/Ag	Re	1.08	21.5	75	17.3	2
		Fw	-	-	-	13.2	
2016	FTO/c-TiO_2/mp-TiO_2/$\mathbf{Cs_{0.2}FA_{0.8}PbI_{2.84}Br_{0.16}}$/Spiro/Au	Re	1.07	21.9	74.2	17.35	3
		Fw	-	-	-	-	
2016	FTO/SnO_2/PCBM/$\mathbf{Cs_{0.17}FA_{0.83}Pb(I_{0.6}Br_{0.4})_3}$/Spiro/Ag	Re	1.20	19.4	75.1	17.10	4
		Fw	-	-	-	-	
2016	FTO/SnO_2/C_{60}-SAM/$\mathbf{Cs_{0.2}FA_{0.8}PbI_3}$/Spiro/Au	Re	1.09	22.25	80.85	19.57	5
		Fw	1.05	22.01	78.25	18.12	
2017	FTO/PCBCB/$\mathbf{Cs_{0.17}FA_{0.83}Pb(I_{0.8}Br_{0.2})_3}$/Spiro/Au	Re	1.07	22.1	80	18.80	6
		Fw	-	-	-	-	
2017	FTO/c-TiO_2/PCBM/$\mathbf{Cs_{0.1}FA_{0.9}PbI_{2.865}Br_{0.135}}$/Spiro/Au	Re	1.04	23	80.5	19.30	7
		Fw	1.01	23.2	73.5	17.20	
2017	FTO/SnO_2/PCBM/$\mathbf{BA_{0.09}(Cs_{0.17}FA_{0.83})_{0.95}Pb(I_{0.6}Br_{0.4})_3}$/Spiro/Au	Re	1.18	19.8	73	17.20	8
		Fw	1.17	19.9	65	15.30	
2017	FTO/c-TiO_2/$\mathbf{BA{:}Cs_{0.15}FA_{0.85}Pb(I_{0.73}Br_{0.27})_3}$/Spiro/Au	Re	1.24	19.83	73.7	18.13	9
		Fw	1.24	19.77	64.1	15.71	
2017	FTO/SnO_2/C_{60}-SAM/$\mathbf{Cs_{0.2}FA_{0.8}Pb(I_{0.7}Br_{0.3})_3}$/Spiro/Au	Re	1.25	18.53	78.95	18.27	10
		Fw	1.21	18.54	74.40	16.62	
2018	FTO/c-TiO_2/$\mathbf{Cs_{0.2}FA_{0.8}Pb(I_{0.95}Br_{0.05})_3}$/Spiro/Au	Re	1.12	22.82	78.82	20.05	11
		Fw	1.08	22.61	74.78	18.20	
2018	FTO/c-TiO_2/mp-TiO_2/$\mathbf{(FAPbI_3)_{0.88}(CsPbBr_3)_{0.12}/(5\text{-}AVA)_2PbI_4}$/CuSCN/Au	Re	1.07	21.93	72	16.75	12
		Fw	1.02	21.89	67	14.97	
2018	FTO/c-TiO_2/$\mathbf{Cs_{0.17}FA_{0.83}Pb(I_{0.6}Br_{0.4})_3}$/Spiro/Au	Re	1.23	18.34	79	17.80	13
		Fw	-	-	-	-	
2018	FTO/c-TiO_2/$\mathbf{Sb^{3+}{:}Cs_{0.1}FA_{0.9}PbI_3}$/Spiro/Ag	Re	1.10	22.85	84	21.04	14
		Fw	1.09	22.83	83	20.65	
2018	FTO/SnO_2/PCBM/PMMA/$\mathbf{Cs_{0.1}Rb_{0.05}FA_{0.85}PbI_3}$/PMMA/Spiro/Au	Re	1.08	25.06	75.5	20.44	15
		Fw	1.05	24.91	70.0	20.35	
2018	FTO/SnO_2/$\mathbf{Cs_{0.17}FA_{0.83}PbI_{2.7}Br_{0.3}}$/Spiro/Au	Re	1.14	23.2	80	21.10	16
		Fw	-	-	-	-	
2018	FTO/EDTA-SnO_2/$\mathbf{Cs_{0.05}FA_{0.95}PbI_3}$/Spiro/Au	Re	1.11	24.57	79.2	21.60	17
		Fw	1.11	24.55	78.3	21.34	
2019	FTO/TiO_2/C_{60}/$\mathbf{FA_{0.9}Cs_{0.1}PbI_3}$/Spiro/Au	Re	0.99	22.32	74.82	16.39	18
		Fw	0.98	22.24	70.54	15.50	
2019	FTO/c-TiO_2/mp-TiO_2/$\mathbf{CEA_{0.05}(Cs_{0.1}FA_{0.9})_{0.95}Pb(I_{0.9}Br_{0.1})_3}$/Spiro/Au	Re	1.10	22.77	79.91	20.08	19
		Fw	1.09	22.48	79.73	19.53	
2019	FTO/ZnO/$\mathbf{Cs_{0.17}FA_{0.83}Pb(I_{0.83}Br_{0.17})_3}$/Spiro/Ag	Re	1.20	22.50	78.1	21.10	20
		Fw	-	-	-	-	
2019	FTO/c-TiO_2/mp-TiO_2/$\mathbf{(Cs_{0.05}FA_{0.95}PbI_3)_{0.94}(CsPbBr_3)_{0.06}}$/Spiro/Au	Re	1.15	24.52	77.5	21.78	21
		Fw	1.15	24.47	72.9	20.54	
2019	FTO/c-TiO_2/mp-TiO_2/$\mathbf{Cs_{0.2}FA_{0.8}PbI_{2.64}Br_{0.36}}$/Carbon	Re	1.08	20.1	66.4	14.50	22
		Fw	1.05	20.1	58.5	12.3	
2020	FTO/c-TiO_2/mp-TiO_2/mp-	Re	0.92	23.63	69	15.00	23

	ZrO_2/$\mathbf{Cs_{0.1}FA_{0.9}PbI_3}$/Carbon	Fw	-	-	-	-	
2020	FTO/c-TiO_2/mp-TiO_2/$\mathbf{HMII\text{-}FAPbI_3}$/Spiro/Au	Re	1.07	24.85	78	20.60	24
		Fw	-	-	-	-	
2020	ITO/SnO_2/$\mathbf{(EDACl_2)_{\omega}(Cs_{0.15}FA_{0.85}PbI_3)}$/Spiro/Ag	Re	1.15	24.11	71.05	19.68	25
		Fw	1.15	23.50	72.60	19.57	
2020	FTO/c-TiO_2/$\mathbf{Cs_{0.15}FA_{0.85}Pb(I_{0.9}Br_{0.1})_3}$-PbS/Spiro/Au	Re	1.15	23.06	79.82	21.07	26
		Fw	1.12	23.07	77.55	20.07	
2020	FTO/SnO_2/$\mathbf{FAPbI_3{:}PbS}$/Spiro/Au	Re	1.11	21.5	75.7	18.00	27
		Fw	-	-	-	-	
2020	FTO/c-TiO_2/$\mathbf{Cs_{0.15}FA_{0.85}Pb(I_{0.9}Br_{0.1})_3}$(Cl)/Spiro/Au	Re	1.18	22.57	80.09	21.30	28
		Fw	1.14	22.74	77.47	20.11	
2020	FTO/c-TiO_2/mp-TiO_2/SnO_2/$\mathbf{Cs_{0.17}FA_{0.83}Pb(I_{0.82}Br_{0.15}Cl_{0.03})_3}$/Spiro/Au	Re	1.12	23.28	78.33	20.50	29
		Fw	-	-	-	-	
2020	FTO/SnO_2/ZnO/$\boldsymbol{\beta}$**-GUA-**$\mathbf{Cs_{0.05}FA_{0.95}PbI_3}$/Spiro/Au	Re	1.14	24.41	79.60	22.2	30
		Fw	-	-	-	-	
2021	FTO/c-TiO_2/$\mathbf{Cs_{0.15}FA_{0.85}Pb(I_{0.95}Br_{0.017}Cl_{0.033})_3}$/Spiro/Au (1.56 eV)	Re	1.16	23.54	81.97	22.4	This work
		Fw	1.14	23.52	78.78	21.1	
2021	FTO/c-TiO_2/$\mathbf{Cs_{0.15}FA_{0.85}Pb(I_{0.7}Br_{0.3})_3}$/Spiro/Au (1.73 eV)	Re	1.24	20.55	78.96	20.2	This work
		Fw	1.21	20.52	77.28	19.1	

Table S2. Parameters of the TRPL spectroscopy based on different samples.

Samples	τ_{ave} (ns)	τ_1 (ns)	τ_2 (ns)	A_1	A_2
Glass/perovskite	537	9.86	544.4	0.44	0.57
Glass/perovskite with PA	901	9.64	905.9	0.35	0.62

Table S3. EIS parameters of the devices based on perovskite films without and with PA.

Devices	R_{tr} (Ω)	CPE1 (F)	R_{rec} (Ω)	CPE2 (F)
Control	145834	7.45E-9	1.374E6	0.4289E-6
PA	91585	8.364E-9	1.646E6	0.530E-6

Table S4. Time evolution of the photovoltaic parameters for PSCs with and without PA.

Samples	Time (days)	V_{OC} (V)	J_{SC} (mA cm^{-2})	FF (%)	PCE (%)
Control	0	1.07904	23.80471	77.36365	19.81106
	1	1.08121	23.72295	78.03683	20.01612
	3	1.09332	23.51503	78.19045	20.10241
	5	1.09961	23.78255	77.5248	20.27398
	7	1.10179	23.77414	77.86444	20.2697
	14	1.10712	23.92551	78.57377	20.67897
	30	1.09937	23.62958	78.33896	20.35068
	60	1.10173	23.57684	78.06763	20.32469
	90	1.10169	23.79391	77.46431	20.3061
	120	1.09753	23.64948	77.45863	20.10513
	150	1.09506	23.70025	77.1592	20.01212
	185	1.09096	23.8125	76.9952	20.00223
	230	1.08806	23.77307	76.27381	19.72148
	275	1.08739	23.83231	75.61594	19.58523
	320	1.08324	23.63445	76.12541	19.48487
	365	1.08026	23.65548	75.35727	19.25064
PA containing perovskite	0	1.11583	23.65242	79.68947	20.96735
	1	1.12535	23.83732	79.59483	21.35151
	3	1.13293	23.23396	80.94256	21.49067
	5	1.13063	23.58939	81.05651	21.6353
	7	1.13952	23.75749	80.52931	21.79367
	14	1.14528	23.79206	80.85145	22.02336
	30	1.13688	23.72214	80.65464	21.75335
	60	1.13186	23.74904	80.37531	21.65477
	90	1.12917	23.6918	80.69422	21.57912
	120	1.12949	23.77144	79.81948	21.43181
	150	1.1275	23.70803	80.34607	21.4833
	185	1.12106	23.69918	80.78639	21.46087
	230	1.11955	23.63145	79.99211	21.1706
	275	1.11512	23.70797	79.8003	21.09635
	320	1.11344	23.69683	79.79206	21.0438
	365	1.10781	23.60874	79.71813	20.8544

References:

1 J.-W. Lee, D.-H. Kim, H.-S. Kim, S.-W. Seo, S. M. Cho and N.-G. Park, *Adv. Energy Mater.*, 2015, **5**, 1501310.

2 Z. Li, M. Yang, J.-S. Park, S.-H. Wei, J. J. Berry and K. Zhu, *Chem. Mater.*, 2016, **28**, 284.

3 C. Yi, J. Luo, S. Meloni, A. Boziki, N. Ashari-Astani, C. Grätzel, S. M. Zakeeruddin, U. Röthlisberger and M. Grätzel, *Energy Environ. Sci.*, 2016, **9**, 656.

4 D. P. McMeekin, G. Sadoughi, W. Rehman, G. E. Eperon, M. Saliba, M. T. Horantner, A. Haghighirad, N. Sakai, L. Korte, B. Rech, M. B. Johnston, L. M. Herz and H. J. Snaith, *Science*, 2016, **351**, 151.

5 Y. Yu, C. Wang, C. R. Grice, N. Shrestha, J. Chen, D. Zhao, W. Liao, A. J. Cimaroli, P. J. Roland, R. J. Ellingson and Y. Yan, *ChemSusChem*, 2016, **9**, 3288.

6 D. P. McMeekin, Z. Wang, W. Rehman, F. Pulvirenti, J. B. Patel, N. K. Noel, M. B. Johnston, S. R. Marder, L. M. Herz and H. J. Snaith, *Adv. Mater.*, 2017, **29**, 1607039.

7 W. Qiu, A. Ray, M. Jaysankar, T. Merckx, J. P. Bastos, D. Cheyns, R. Gehlhaar, J. Poortmans and P. Heremans, *Adv. Funct. Mater.*, 2017, **27**, 1700920.

8 Z. Wang, Q. Lin, F. P. Chmiel, N. Sakai, L. M. Herz and H. J. Snaith, *Nat. Energy*, 2017, **2**, 17135.

9 Y. Zhou, F. Wang, Y. Cao, J.-P. Wang, H.-H. Fang, M. A. Loi, N. Zhao and C.-P. Wong, *Adv. Energy Mater.*, 2017, 1701048.

10 Y. Yu, C. Wang, C. R. Grice, N. Shrestha, D. Zhao, W. Liao, L. Guan, R. A. Awni, W. Meng, A. J. Cimaroli, K. Zhu, R. J. Ellingson and Y. Yan, *ACS Energy Lett.*, 2017, **2**, 1177.

11 Y. Wu, P. Wang, S. Wang, Z. Wang, B. Cai, X. Zheng, Y. Chen, N. Yuan, J. Ding and W.-H. Zhang, *ChemSusChem*, 2018, **11**, 837.

12 J. Chen, J.-Y. Seo and N.-G. Park, *Adv. Energy Mater.*, 2018, 1702714.

13 J. Kim, M. I. Saidaminov, H. Tan, Y. Zhao, Y. Kim, J. Choi, J. W. Jo, J. Fan, R. Quintero-Bermudez, Z. Yang, L. N. Quan, M. Wei, O. Voznyy and E. H. Sargent, *Adv. Mater.*, 2018, **30**, 1706275.

14 H. W. Qiao, S. Yang, Y. Wang, X. Chen, T. Y. Wen, L. J. Tang, Q. Cheng, Y. Hou, H. Zhao and H. G. Yang, *Adv. Mater.*, 2018, **30**, 1804217.

15 S.-H. Turren-Cruz, A. Hagfeldt and M. Saliba, *Science*, 2018, **362**, 449.

16 Z. Wang, Q. Lin, B. Wenger, M. G. Christoforo, Y.-H. Lin, M. T. Klug, M. B. Johnston, L. M. Herz and H. J. Snaith, *Nat. Energy*, 2018, **3**, 855.

17 D. Yang, R. Yang, K. Wang, C. Wu, X. Zhu, J. Feng, X. Ren, G. Fang, S. Priya and S. Liu, *Nat. Commun.*, 2018, **9**, 3239.

18 J. Chen, J. Xu, C. Zhao, B. Zhang, X. Liu, S. Dai and J. Yao, *ACS Appl. Mater. Interfaces*, 2019, **11**, 4597.

19 G. Liu, H. Zheng, X. Xu, S. Xu, X. Zhang, X. Pan and S. Dai, *Adv. Funct. Mater.*, 2019, **29**, 1807565.

20 K. Schutt, P. K. Nayak, A. J. Ramadan, B. Wenger, Y.-H. Lin and H. J. Snaith, *Adv. Funct. Mater.*, 2019, 1900466.

21 L. Xie, K. Lin, J. Lu, W. Feng, P. Song, C. Yan, K. Liu, L. Shen, C. Tian and Z. Wei, *J. Am. Chem. Soc.*, 2019, **141**, 20537.

22 Z. Wu, Z. Liu, Z. Hu, Z. Hawash, L. Qiu, Y. Jiang, L. K. Ono and Y. Qi, *Adv. Mater.*, 2019, **31**, 1804284.

23 X. Hou, M. Xu, C. Tong, W. Ji, Z. Fu, Z. Wan, F. Hao, Y. Ming, S. Liu, Y. Hu, H. Han, Y. Rong and Y. Yao, *J. Power Sources*, 2019, **415**, 105.

24 S. Akin, E. Akman and S. Sonmezoglu, *Adv. Funct. Mater.*, 2020, **30**, 2002964.

25 J. Hou, F. Deng, Q. Wu, L. Yang, J. Wu, X. Li, Y.-Z. Zheng, N. Li, H. Ding and X. Tao, *J. Power*

Sources, 2020, **449**, 227484.

26 Y. Chen, J. Yang, S. Wang, Y. Wu, N. Yuan and W.-H. Zhang, *iScience*, 2020, **23**, 100762.

27 S. Masi, C. Echeverría-Arrondo, K. M. M. Salim, T. T. Ngo, P. F. Mendez, E. López-Fraguas, D. F. Macias-Pinilla, J. Planelles, J. I. Climente and I. Mora-Seró, *ACS Energy Lett.*, 2020, **5**, 418.

28 J. Yang, Y. Chen, W. Tang, S. Wang, Q. Ma, Y. Wu, N. Yuan, J. Ding and W.-H. Zhang, *J. Energy Chem.*, 2020, **48**, 217.

29 X.-X. Gao, W. Luo, Y. Zhang, R. Hu, B. Zhang, A. Züttel, Y. Feng and M. K. Nazeeruddin, *Adv. Mater.*, 2020, **32**, 1905502.

30 Q. Yao, Q. Xue, Z. Li, K. Zhang, T. Zhang, N. Li, S. Yang, C. J. Brabec, H.-L. Yip and Y. Cao, *Adv. Mater.*, 2020, **32**, 2000571.